EP challenge - STACOM'11: forward approaches to computational electrophysiology using MRI-based models and in-vivo CARTO mapping of swine hearts

Mihaela Pop[1], Maxime Sermesant[2], Tommaso Mansi[3], Eugene Crystal[1], Sudip Ghate[1], Jatin Relan[2], Charles Pierre[4], Yves Coudiere,[5], Jennifer Barry[1], Ilan Lashevsky[1], Beiping Qiang[1], Elliot R McVeigh[6], Nicholas Ayache[2], Graham A Wright[1]

mihaela.pop@utoronto.ca and gawright@sri.utoronto.ca

[1]Sunnybrook Research Institute, University of Toronto, Canada, [2]INRIA - Asclepios project, Sophia-Antipolis, France, [3]Siemens Corporate Research, Princeton, NJ, USA, [4]University of Pau, France, [5]Inst. Mathematiques de Bordeaux; France, [6]Johns Hopkins University, Baltimore, USA

Abstract. Our broad aim is to integrate experimental measurements (electro-cardiographic and MR) and cardiac computer models, for a better understanding of transmural wave propagation in individual hearts. In this paper, we first describe the acquisition and processing of the data provided to the EP simulation challenge organized at STACOM'11. The measurements were obtained in two swine hearts (i.e., one healthy and one with chronic infarction) and comprise in-vivo electro-anatomical CARTO maps (e.g., surfacic endo-/epicardial depolarization maps and bipolar voltage maps recorded in sinus rhythm), and high-resolution ex-vivo diffusion-weighted DW-MR images (voxel size $< 1mm^3$). We briefly detail how we built anisotropic 3D MRI-based models for these two hearts, with fiber directions obtained using DW-MRI methods (which also allowed for infarct identification). We then focus on applications in cardiac modelling concerning propagation of depolarization wave, by employing forward mathematical approaches. Specifically, we present simulation results for the depolarization wave using a fast, macroscopic monodomain formalism (i.e., the two-variable Aliev-Panfilov model) and comparisons with measured depolarization times. We also include simulations obtained using the healthy heart and a simple Eikonal model, as well as a complex bidomain model. The results demonstrate small differences between computed isochrones using these computer models; specifically, we calculated a mean error $\pm$ S.D. of 2.8 ± 1.67 ms between Aliev-Panfilov and Eikonal models, and 6.1 ± 3.9 ms between Alie-Panfilov and bidomain models, respectively.

Keywords: electrophysiology, 3D computer modelling, cardiac DW-MRI

1 Introduction:

Abnormal rhythms (arrhythmias) are often associated with abnormal propagation of electrical wave in hearts with structural disease and are a major cause (>85%) of sudden cardiac death [1]. Currently, chronic infarct areas are identified during the electrophysiology (EP) study using for instance the CARTO-XP electro-anatomical system (Biosense, Diamond, USA). This system is limited to surfacic endocardial and/or epicardial maps obtained invasively via catheters inserted into the heart cavities, under fluoroscopy. However, many patients are hemodynamically unstable

and therefore the scar mapping is done only during the sinus rhythm; only very established clinical centers map the patients under pacing conditions. Thus, there is a strong clinical motivation to supplement the electrophysiology measurements with non-invasive information, like 3D anatomy and accurate scar delineation. Should this information is known, image-based predictive computer models could be integrated in treatment planning platforms and help the clinician improve therapy through identification of strategies most appropriate to the individual patient [2]. Hence, an important task is to find the location, extent and transmurality of the scar in post-infarction patients. Clinically, this is done non-invasively with contrast-enhanced (c-e) MRI methods; however, identification of infarcted areas suffers from partial volume effects due to the slice thickness (~ 8 mm) [3]. Other methods, like non-contrast MR could be exploited, particularly those that allow extraction of fiber directions. For instance, using diffusion-weighted DW-MRI methods, it was demonstrated in ex-vivo formalin-fixed porcine hearts studies that scars correspond with the regions of increased apparent diffusion coefficient (ADC) [4]. Similar findings were observed in-vivo, in patients with prior myocardial infarct, but these MR scans are in general of poor resolution because motion artifacts significantly affect in-vivo imaging [5].

In addition to standard clinical evaluations using EP studies and MR imaging, computer modelling has been extensively used in cardiac electrophysiology to predict the heart's electrical activity [6,7]. Recent progress has demonstrated that image-based computer models can be integrated in treatment planning platforms [2]. However, prior to integration into routine clinical applications, such predictive models have to be validated/calibrated using experimental techniques selected to reflect EP phenomena at spatio-temporal scales similar to those in simulations. Importantly, these cardiac computer models need to account for myocardial tissue anisotropy; here the fiber directions are obtained via ex-vivo DW-MRI or atlases. Other groups focused to construct image-based models from normal and pathologic large animal hearts, with size relevant to human hearts. Some applications concerned simulations of virtual cases of arrhythmias using complex computer models built from noisy fractional anisotropy maps of dog hearts; although the results were encouraging, the studies lacked experimental validation [8]. Our group combined simplified 3D MRI-based computer models with electrophysiology measures from optical fluorescence imaging, to validate the propagation and characteristics of action potential, as well as to customize several model parameters in large healthy hearts, ex-vivo [9, 10]. However, our final aim is to characterize post-infarction chronic scars using realistic in-vivo EP measures augmented with accurate 3D information from high-resolution ex-vivo MRI imaging, and also to complement this knowledge with insights from theoretical modeling. The first step in achieving this goal is the development of a pre-clinical large-heart model that could characterize cardiac electrical and structural function with sufficient information, at least at a macroscopic level. This should allow us to perform accurate validation and parameterization of computer models on a heart-basis, as well as to test various mathematical approaches of different degree of complexity, and test the utility and performance of associated computer models.

We believe that the development of experimental datasets and sharing data and results within the community, will advance us toward this goal by addressing the

advantages and limitations of different mathematical models. One step forward in this direction was already taken for the last year's EP simulation challenge at STACOM-CESC'10, where the participants have tested and/or calibrated their computer models using experimental datasets published in [9, 10]. These datasets comprised ex-vivo optical fluorescence images (isochronal maps of depolarization and repolarization phase) fused with ex-vivo DW-MR images of healthy swine hearts. A review paper [11] included the results from all challenge participants, focusing on consistency and main complementarities between various modelling approaches proposed by these research groups.

The next logical step is to advance such efforts towards the applications concerning in-vivo EP measurements. This current challenge paper describes first in detail the data acquisition and processing for the EP simulation challenge organized at STACOM'11, where we provided the challengers with experimental datasets (in-vivo EP and ex-vivo MRI) obtained in healthy and chronically infarcted swine hearts. We then present applications in computational electrophysiology using the two 3D MRI-based heart models (healthy and pathologic) and forward (direct) mathematical approaches. Specifically, we include simulation results for the depolarization wave using a simple macroscopic, monodomain formalism (i.e., the two-variable Aliev-Panfilov model), as well as qualitative and quantitative comparisons with the measurements. We investigate if, for applications concerning only computations of the electrical wave propagation, this two-variable model is sufficient, and, for this, include comparisons between simulation results obtained with Aliev-Panfilov model, and simulation results obtained using other formalisms: the simplest model (i.e., Eikonal model) and a complex model (i.e., bidomain model).

2   EP-CARTO and DW-MRI data acquisition and processing

We describe below the experimental steps following the order in which they were performed. We first completed the in-vivo EP studies. We then explanted the hearts and used DW-MRI to measure the myocardial fiber directions and delineate the infarct. These MR images were further used to build 3D heart computer models.

2.1 In-vivo electrophysiology study and ex-vivo MRI study

For the EP simulation challenge organized at STACOM'11, we included two cases in which the in-vivo EP study was performed in accordance to the animal protocol in a pre-clinical swine model approved by Sunnybrook Research Institute (Toronto, Canada). All electrophysiology maps described in this paper were recorded in sinus rhythm with the CARTO-XP electro-anatomical mapping system (Biosense, Diamond, USA). Specifically, the EP studies were performed in: a healthy swine, and a swine that had a 5-week old chronic infarct. For the pathologic case, the infarction was generated by occluding the left circumflex artery (LCX) for 90'-min with a balloon catheter; this was followed by the retraction of the balloon, reperfusion of the LCX-territory and scar healing.

Figure 1 shows representative images taken during an in-vivo EP study in the infarcted heart. Fig 1a shows the EP catheter inserted into the cavity of LV of LCX-infarct heart, under fluoroscopy guidance. Figure 1b shows the location of each recorded point on a raw mesh reconstructed with the CARTO-XP analysis software. Figure 1c shows the reconstructed isochronal map of the LV-epicardium (isochrones 5 ms apart) with latest activation time points in blue and the earliest points in red. For each recorded point, the following information was stored: precise geometrical location (via the X, Y, Z coordinates), unipolar values, bipolar voltage values, early activation times (EAT), late activation times (LAT). From these recordings, isochronal maps of the depolarization phase can be constructed and displayed, or exported to other software tools for further analysis.
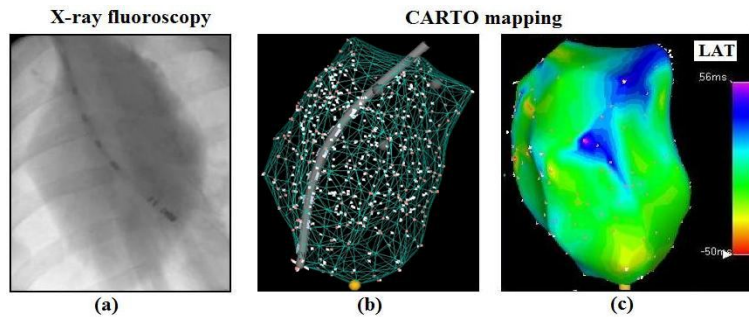
Fig. 1 The in-vivo EP study in the LCX-infarct heart: (a) recording EP catheter viewed under X-ray fluoroscopy, during its guidance into LV cavity for LV-endocardial mapping; (b) anatomical positions of the LV-endocardial CARTO points and associated mesh; and (c) reconstructed LV endocardial isochronal map (with the isochrones of depolarization times shown 5 ms apart).

At the completion of the EP studies, the hearts were explanted, gently preserved in formalin, and imaged using a 1.5Tesla SignaExcite GE MR scanner for anatomy, myocardial fiber directions previously described in [9, 12], and scar delineation. For these two hearts we used the following MR parameters: TE = 32 ms, TR = 700 ms, NEX=1, *b*-value ~ 700 (for healthy heart) and ~500 (for LCX-infarct heart), 7 directions for diffusion gradients, FOV/matrix = 10 cm, 256x256 acquisition matrix (yielding a 0.5 mm x 0.5 mm in plane spatial resolution), and an approximately 1.5 - 1.8mm slice thickness.

Figure 2a shows the in-vivo electro-anatomical voltage maps (EAVM) calculated from bipolar maps recorded in the LCX-infarct heart on the LV-endocardium and epicardium. To delineate the scar in these CARTO bipolar voltage maps, we used clinical cut-off threshold voltage values < 1.5 mV; note that this threshold included dense infarct scar and peri-infarct areas (found at the border zone between dense scar and healthy myocardium). Figure 2b shows a 2D ex-vivo long-axis DW-MR image through this heart; elevated values of apparent diffusion coefficient (ADC-MRI) in the infarct areas are observable in the LCX territory. Very good correspondence was observed between the location and extent of the infarct area identified in both EP-CARTO maps and DW-MR images.
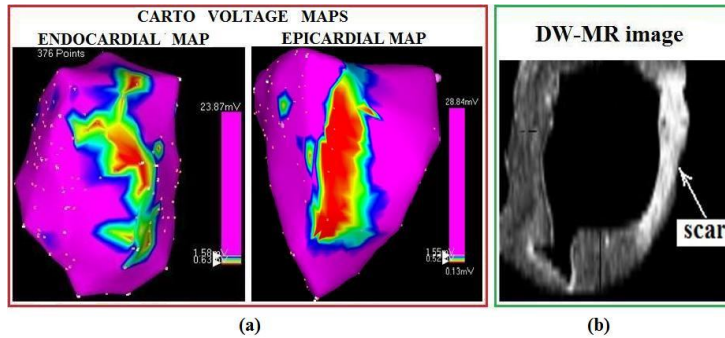
Fig. 2 Scar identification and characterization for the LCX-infarcted heart: (a) scar delineated in the endocardial EAVM (left) and epicardial EAVM (right) from bipolar maps; and b) a 2D long-axis view in an MR image with the scar delineated by the elevated (i.e., bright) ADC values compared to the values in remote, healthy tissue.

2.2 Fiber directions from DW-MRI and histological evaluation of the scar

For both hearts, fiber directions for their corresponding anisotropic models were estimated from the first Eigen vectors, using reconstructed diffusion tensor images. Figure 3 shows the reconstructed fiber directions for both hearts.
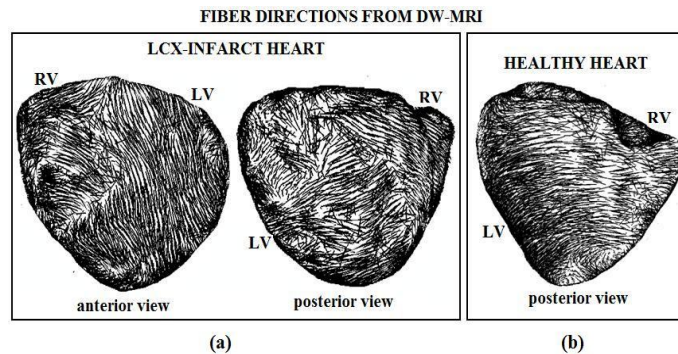
Fig. 3 Fiber directions from DW-MRI in the: (a) LCX-infarct heart; and (b) healthy heart.

Histopathological analysis using Picrosirius Red stain in the LCX-infarct heart demonstrated dense collagen deposition, replacement of dead myocytes by fibrosis and severe alteration in myocardial tissue architecture in the infarct area. Figure 4 shows a 2D short-axial image through the 3D DW-MRI volume, that matched the corresponding histological samples taken from the scarred tissue and from a remote healthy area in the LV-endocardium of the LCX-infarcted heart. The stained slide was then scanned at a 5-micron resolution, using an Aperio-ImageScope system and saved as multi-resolution digital image.
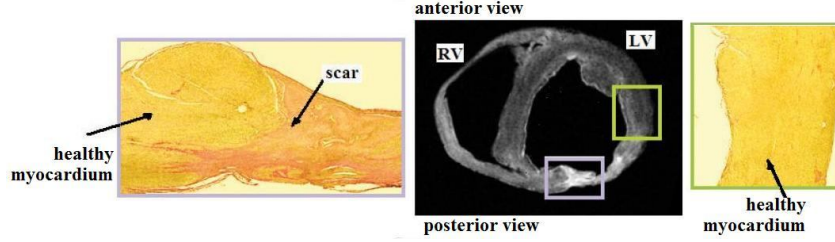
Fig. 4 Chronic infarct scar identified in the DW-MRI image and corresponding histological slide using Picrosirius Red stain that demonstrated collagen deposition (in red), with fibrosis in the infarct area replacing dead myocytes.

For the construction of the 3D heart models, the anatomy of each heart was extracted from the un-weighted images (i.e., b=0) and then used to generate masks and volumetric meshes for the mathematical model; fiber directions were also integrated in these meshes. For the LCX-infarct heart, the 3D apparent diffusion coefficient (ADC) maps were further used to segment this heart into two zones: healthy tissue and infarct area (note that the latter is electrically inert and does not propagate electrical wave).

3 Forward problems applied to computational electrophysiology

3.1 A simple macroscopic two-variable modelling approach

We used the macroscopic Aliev-Panfilov model, which is based on reaction-diffusion type of equations, and has a monodomain approach (i.e., the intra- and extracellular spaces are collapsed into each other and represented by "bulk" tissue properties) as described in [13]. The term $-kV(V-a)(V-1)$ controls the fast processes (initiation and upstroke of action potential, AP) via the threshold parameter a, while r, determines the dynamics of the repolarization phase. In the system of equations (1)-(2) we solve for the AP, here noted V. We use Finite Element Methods, with an explicit Euler time integration scheme, as implemented in [14].

$$\frac{\partial V}{\partial t} = \nabla \cdot (D\nabla V) - kV(V-a)(V-1) - rV \qquad (1)$$

$$\frac{\partial r}{\partial t} = -(\varepsilon + \frac{\mu_1 r}{\mu_2 + V})(kV(V-a-1)+r) \qquad (2)$$

This simple two-variable model accounts for heart anisotropy via the diffusion tensor D (which depends on tissue 'bulk' conductivity, d). The anisotropy ratio is set to 0.25 for a wave propagating twice as fast along the fibers. The values for model's input parameters were assigned as in [15]; d was set to zero in the infarct scar (i.e., the electrical wave does not propagate through this scar zone).

The 3D-heart model (anatomy and scar) of the LCX-infarct heart is shown in Fig 5a. The simulation results for this heart were achieved as follows: the normal sinus rhythm was simulated by applying a square pulse of 5 ms seconds and maximum amplitude (i.e., $V = 1$, since the output has normalized values for AP). In the absence of realistic Purkinje fibers integrated in the model, this stimulus was applied on the endocardium (at the apex) to mimic a normal activation wave, with an apex-to-base propagation. Note that in the CARTO-endocardial maps we identified a conduction block on the septum of left ventricle with an LBBB morphology, which was mimicked by applying the stimulus only at the RV-apex (see red dot in Fig. 5b). Figure 5c shows the simulated depolarization map (lateral-posterior view of the epicardium, with scar in black), with early depolarization times in red and late activation times in blue. Figures 5d and 5e show the experimental endocardial and epicardial isochronal maps (in a lateral-posterior view) projected onto the mesh, whereas Fig. 5f shows the error in activation times (i.e., absolute difference between measured and simulated depolarization times).
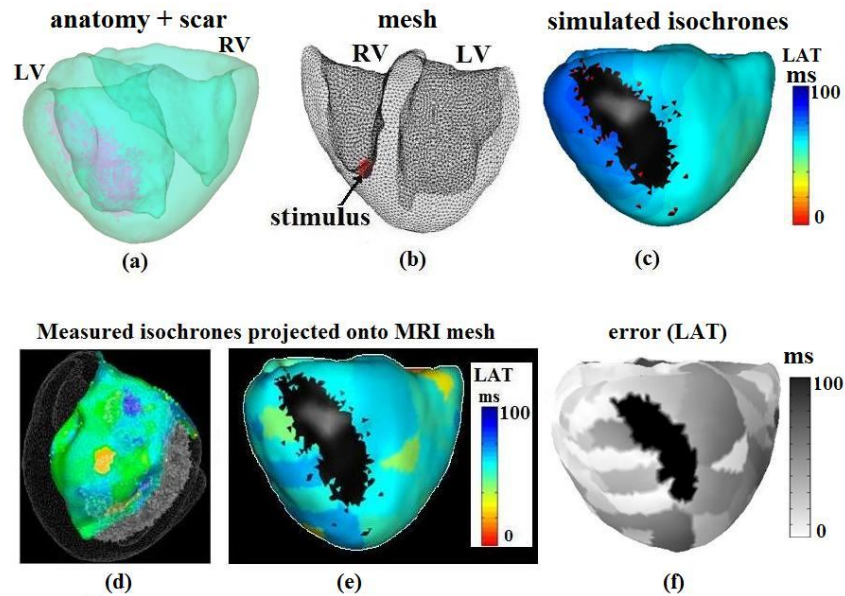
Fig. 5 Results obtained using the image-based model built for the LCX-infarct heart: (a) the 3D MRI-based heart model; (b) the location where the stimulus was applied at the apex of the RV-endocardium; (c) simulated isochrones of depolarization phase represented by LAT times (ms), displayed in a lateral-view. Corresponding experimental isochronal maps projected onto: (d) LV-endocardium, (e) epicardium; and (f) absolute error between the measured depolarization times on the epicardium and corresponding map of simulated depolarization times (ms).

Figure 6 shows a good correspondence between experimental and simulated isochronal maps of depolarization times, for the healthy heart. Experimental isochrones are represented from the RV-endocardium (Fig 6a), for LV-endocardium (Fig 6b), as well the epicardial maps (Fig 6c), all maps have early depolarization times in red, and latest activation times, LAT, in blue. The black points in Fig 6d (cross-section view through the heart) represent the locations where the stimuli (square pulse, $V = 1$) were applied in the 3D MRI-based computer model (selected on the endocardium of RV and LV); these points closely reproduced the locations of early activation points determined from experimental endocardial maps. The resulting epicardial breakthrough, had similar pattern and timing in experiment and simulations.
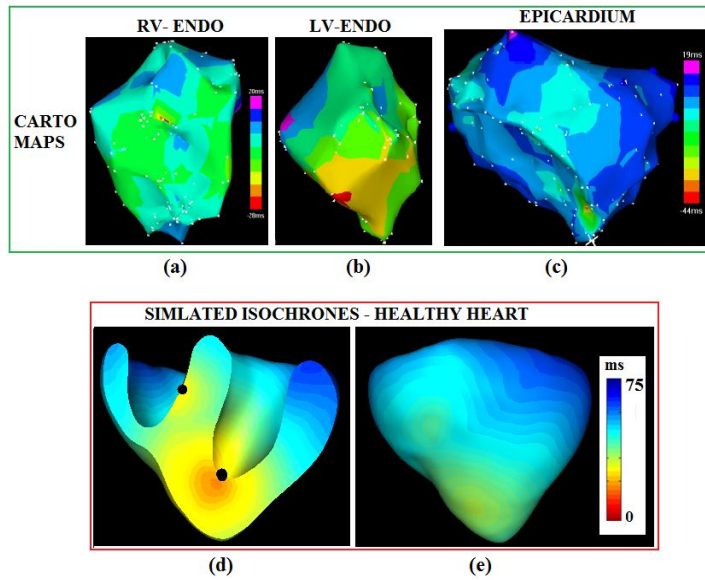
Fig. 6 Experimental (a-c) and simulation (d-e) results obtained in the healthy heart.

For the Aliev-Panfilov model, when using time steps of 5×10^{-5}s, the simulation time of 0.8s of the heart cycle on a mesh of approximately 190,000 elements (with an average element size of approximately 1.2 mm), is about 40 min on an Intel ® Core™ 2 duo CPU, T5550 @1.83GHz, with 4 GB of RAM.

3.2. Other mathematical models and computation results of forward problems

We further investigated the feasibility of applying other mathematical approaches to the forward problem, in order to compute the wave propagation. For this, we selected two other well-established models: one simpler than the A-P model (i.e., the Eikonal model) and the other one more complex (i.e., the bidomain model).

The Eikonal model is the simplest and fastest mathematical model used in cardiac electrophysiology [16]; thus, is attractive to clinical applications [2]. It computes only the wave front propagation (i.e., the depolarization phase Td of the electrical wave) based on the anisotropic Eikonal equation (3):

$$v^2\left(\nabla T_d^t D \nabla T_d\right)=1 \tag{3}$$

Where the v is the local speed of the wave and D is the diffusion tensor. In the fiber orientation coordinates, D = diag(1, ρ, ρ), where ρ is the anisotropy ratio between conduction velocity (i.e., speed of wave) in transverse and longitudinal directions.

The bidomain model offers the most complete description of electrical behaviour of myocardium. It explicitly accounts for the current flow in the two spaces (extra-/intercellular) through non-linear PDEs (4) and (5):

$$A_m(C_m(\partial_t V_m + I_{ion}(V_m,y,c)\text{-}I_{stim}(x,t)) = div(G_i \nabla(V_m+\phi_e)) \tag{4}$$

$$div((G_i+G_e)\nabla\phi_e) + div(G_i \nabla V_m)) =0 \tag{5}$$

where V_m is the transmembrane potential, c is ion concentration (/specie), A_m is the cellular surface to volume ratio, Cm is membrane capacitance, G is the conductance of a space extra- or intracellular. The system models these spaces from an electro-static point of view; thus, these equations need to be coupled via a non-linear model that describes the current flow from one space into the other. In this paper, for the computation of this current, we use the model proposed by Tusscher-Noble-Noble-Panfilov described in [17]. For the numerical method and algorithm, the equations are discretized using the P1 Lagrange FEM, and a first order implicit/explicit time-stepping strategy. The evolution of V_m and ϕ_e is solved implicitly using the optimal pre-conditioner defined in [18]. For the boundary conditions of the system (4)-(5), we use the following constraints: $G_i \nabla(V_m+\phi_e)\cdot n = 0$ and $G_e \nabla\phi_e \cdot n = 0$.

Figure 7 shows a comparison of the depolarization times obtained using the three models. For each model, the results are shown in: top-view (Figs 7a, 7d and 7g), longitudinal/transmural cross-section view (Figs 7b, 7e and 7h), and anterior view, respectively (Figs 7c, 7f and 7i). A good agreement between the LATs was observed, along with very small notable differences in the pattern of activation times and epicardial breakthrough. Note that, for these particular set of simulations, in all three models, we started the excitation at the RV-apex and LV-apex on the endocardium. For the A-P and Eikonal models we used an anisotropy ratio of 0.25. For A-P, most parameters were set as in [15] except for $d = 2$ (to tune a speed of wave that resulted in ventricles depolarization within ~92 ms); for the Eikonal model we set a speed of 65 cm/s (along the fiber). For the bidomain model, we used the following conductivities (mS/cm) for the longitudinal & transverse directions, and for the intra-/extracellular spaces: $G_i(l) = 1.741$; $G_i(t) = 0.193$; $G_e(t) = 1.970$ and $G_e(l) = 3.906$. Other membrane characteristics were set to $C_m = 1$ mF/cm^2 and $A_m = 250$ cm^{-1}; an external current of 52 μA/cm^2 was applied to start the depolarization and a time step of 1×10^{-4}s was used to solve explicitly the equations for ion concentrations. The time required to compute 0.2 s of heart cycle using the bidomain model was ~70 min, and less than 1 min for the Eikonal model.
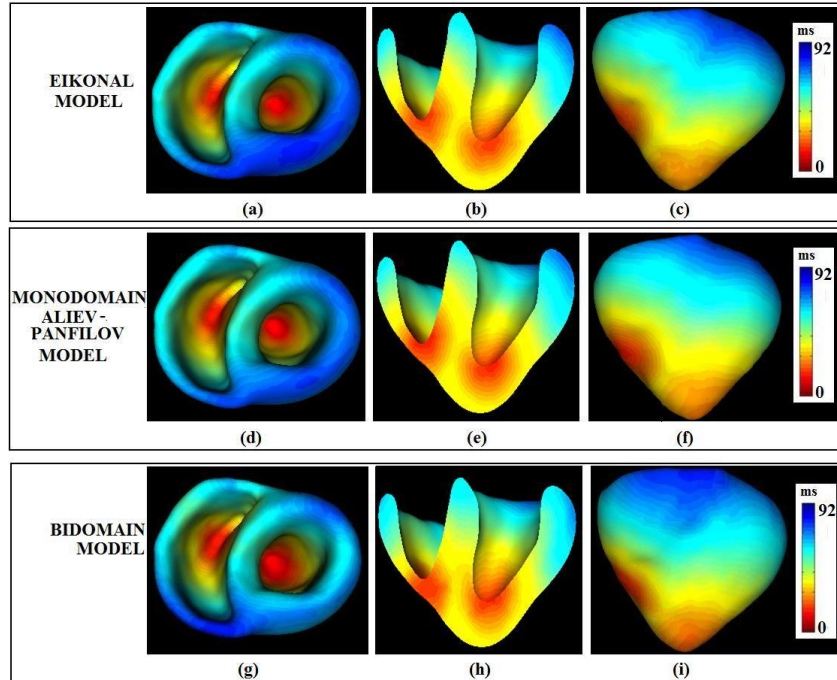
Fig. 7 Comparison between the simulated isochronal maps obtained using: (a-c) the Eikonal model, (d-f) the Aliev-Panfilov model; and (g-i) the Bidomain model (see more details in the text).

The errors between simulated depolarization times obtained using the models are shown in Fig 8. Specifically, for the comparison between Aliev-Panfilov model and Eikonal model, we computed a mean error $\pm$ S.D of 2.76 ± 1.67 ms (calculated over all vertices in the mesh) with an RMS error 7.4 ms. For the comparison between Aliev-Panfilov and bidomain model, we obtained a mean error 6.1 ± 3.9 ms, and a 12.96 ms RMS error.
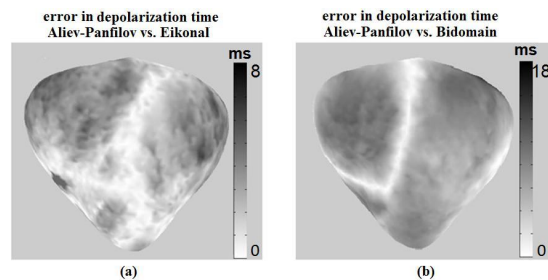
Fig. 8 Absolute difference between computed depolarization times (ms): (a) Aliev-Panfilov vs. Eikonal model; and (b) Aliev-Panfilov vs. Bidomain model.

4. Discussion

Advances leading to improved disease management and therapy planning, as well as outcomes assessment, would have immediate impact on the quality of life in patients with prior myocardial infarction. Integration of EP measures with image-based models is useful because it can help us understand a realistic 3D transmural propagation of the cardiac excitation wave. Thus, current research efforts are focused on improving non-invasive imaging methods, and on developing image-based predictive computer models using forward [8, 9, 11, 20] and inverse problems [2, 10, 19] designed to customize such models. With this respect, sharing experimental data, as well as comparing modelling results between research groups are important milestones; the EP simulation challenge (at STACOM'10 and STACOM'11) represents an excellent joined effort toward achieving this goal.

In this paper, we described in detail several steps undertaken in the development of a pre-clinical framework that integrates experimental in-vivo CARTO data and high-resolution ex-vivo DW-MRI data from the two swine hearts (healthy and with chronic infarction), given to the STACOM'11 participants. The DW-MRI data allowed us to delineate the scar, as well as to determine the fiber directions, which is important to consider for a correct representation of tissue anisotropy. For the modelling part, we presented forward approaches to cardiac modelling and computed only the propagation of depolarization wave. Further, isochronal maps depolarization times were calculated, and then compared with measured depolarization times recorded by EP-CARTO. Our simulation results suggest that the two-variable Aliev-Panfilov model can give a good representation of the wave propagation. In a first approximation, the conductivity parameter d, which tunes the conduction velocity and, consequently, the depolarization times was tuned using a "trial and error" approach. This adjustment of d minimized the errors between simulations and experiments, and resulted in a good correspondence with respect to associated activation patterns and isochronal maps. We acknowledge that a more accurate tuning of model parameters could be performed by: i) partitioning the heart in smaller (AHA) zones, ii) analyzing the infarct heterogeneities (i.e., classify the infarct in scar and border zone), and iii) optimizing the parameters adjustment as per the methods proposed in [10, 19].

Fast predictive models that require short computation times are desirable, particularly for models aiming to be integrated into clinical platforms. Applications of cardiac image-based computer models, limitations, validation, parameterization, as well as accuracy and associated errors between predictions and measurements, are all important. As a preliminary test, for the healthy heart, we included simulations obtained using the simplest model (Eikonal) and a complex model (Bidomain); our results demonstrated small differences between the computed activation pattern and depolarization maps using these three models. In the future, we will design specific tests to demonstrate when simplified models fail to produce satisfactory results, and thus complex models should be used (in particular for modelling the pathologic cases),

To conclude, evaluation of 3D image-based computer models performance and utility, as well as customization using in-vivo EP measurements will help us to use such models correctly, and to properly target them for different applications.

Reference:

1. W.G. Stevenson.: Ventricular scars and VT tachycardia; Trans Am Clin Assoc (2009)120: 403-12.
2. P. Chinchapatnam, K.S. Rhode, M. Ginks, C.A. Rinaldi, P. Lambiase, R. Razavi, S. Arridge, M. Sermesant; Model-Based imaging of cardiac apparent conductivity and local conduction velocity for planning of therapy; IEEE Trans Med Imaging (2008), 27 (11):1631-1642
3. D. Bello, DS Fieno, RJ, Kim RJ et al., Infarct morphology identifies patients with substrate for sustained ventricular tachycardia; J Am College of Cardiology, (2005), 45 (7), 1104-110
4. E.X. Wu, Y. Wu, H. Tang, J. Wang, J. Yang, M Ng, *et al*: MR-DT imaging study of post infarct myocardium; structural remodeling in a porcine model. Magn Res Med (2007), 58 (4), 687–695
5. M.T. Wu, W.Y. Tseng, M.Y. Su, K.R. Chiou, T.G. Reese, C.F. Yang: DT-MRI mapping of fiber architecture remodeling in human myocardium after infarction; Circulation (2006) 114, 1036-1045
6. R.H. Clayton and A.V. Panfilov: A guide to modelling cardiac electrical activity in anatomically detailed ventricles. Progress in Biophysics & Molecular Biology – review; (2008), 96 (1-3) 19-43
7. P.J. Hunter, E.J. Crampin, P.M. Nielsen: Bioinformatics, multi-scale modeling and the IUPS Physiome project.; in Brief Bioinform. (2008) 9 (4): 333-43
8. F. Vadakkumpadan, L. Rantner, B. Tice, P.Boyle, A. Prassl, E. Vigmond, G. Plank, N. Trayanova: Image-based models of cardiac structure with applications in arrhythmia and defibrillation studies, J. Electrocardiology; (2009) 42 (2) 15
9. M. Pop, M. Sermesant, D. Lepiller, M. Truong, E.R. McVeigh, E. Crystal, A.J. Dick, H. Delingette, N. Ayache, G.A.Wright; Fusion of optical imaging and MRI for the evaluation and adjustment of macroscopic models of cardiac electrophysiology: a feasibility study; Medical Image Analysis, (2009) 13(2): 370-80
10. J. Relan, M. Pop, H. Delingette, G.A. Wright, N. Ayache and M. Sermesant; Personalisation of a cardiac electrophysiology model using optical mapping and MRI for prediction of changes with pacing. IEEE Trans Biomed Eng. 2011 Jan 20 (in press)
11. O. Camara, M. Sermesant, P. Lamata, L. Wang, M. Pop, J. Relan, M. De Craene, H. Delingette, H. Liu, S. Niederer, G. Plank A. Pashaei and, D. Romero, R. Sebastian, K.C.L. Wong, H. Zhang, N. Ayache, A.F. Frangi, P. Shi, N.P. Smith, G.A. Wright; Inter-model consistency and complementarity: learning from ex-vivo imaging and electrophysiological data towards an integrated understanding of cardiac physiology**;** Prog. Biophys. Molec. Biol. (2011) in press
12. P. Helm, H.J. Tseng, L. Younes, E.R. McVeigh, R.L. Winslow: Ex-vivo 3D diffusion tensor imaging and quantification of cardiac laminar structure. Magn. Res. Med. (2005) 54, 850-859.
13. R. Aliev and A.V. Panfilov: A simple two variables model of cardiac excitation; Chaos, Soliton and Fractals, (1996), 7(3), 293-301.
14. M. Sermesant, H. Delingette, N. Ayache; An electromechanical model of the heart for image analysis and simulations; IEEE Transaction in Medical Imaging, (2006), 25 (5), 612-625
15. Nash M P, and Panfilov A V: Electromechanical model of excitable tissue to study reentrant cardiac arrhythmias; Prog Biophys Molec Biol 2004, 85, 501-522.
16. J.P. Keener and J. Sneeyd, Mathematical physiology, (1998) Spinger
17. K.H. Ten Tusscher, D. Noble, P.J. Noble, A.V.Panfilov; A model for human ventricular tissue. Am. J. Physiol. Heart Circ. Physiol. (2004) 286 (4)
18. C. Pierre; Preconditioning in bidomain model with almost linear complexity. Journal of Computational Physics (2011), in press
19. E. Konukoglu, J. Relan, U. Cilingir, B. Menze, P. Chinchapatnam, A. Jadidi, H. Cochet, M. Hocini, H.Delingette, P. Jais, M. Haissaguerre, N. Ayache, M Sermesant; Efficient probabilistic model personalization integrating uncertainty on data and parameters: applications to Eikonal-Difusion models in cardiac electrophysiology; Prog. Biophys. Molec Biol (2011) in press.
20. M. Pop, M. Sermesant, T. Mansi, E. Crystal, S. Ghate, J-M Peyrat, I. Lashevsky, B. Qiang, E.R. McVeigh, N. Ayache, G. A. Wright; Correspondence between simple 3D MRI-based computer models and in-vivo EP measurements in swine with chronic infarctions; IEEE Trans. Biomed. Eng. (2011), Vol. 58 (12).